Available online at www.sciencedirect.com
SCIENCE DIRECT®
International Journal of Multiphase Flow 30 (2004) 125–137
International Journal of Multiphase Flow
www.elsevier.com/locate/ijmulflow

Interfacial measurements in stratified types of flow. Part II: Measurements for R-22 and R-410A

Leszek Wojtan, Thierry Ursenbacher, John R. Thome *

Laboratory of Heat and Mass Transfer (LTCM), Faculty of Engineering Science (STI), Swiss Federal Institute of Technology Lausanne (EPFL), CH-1015 Lausanne, Switzerland

Received 20 January 2003; received in revised form 24 November 2003

Abstract

A new optical void fraction measurement system has been coupled to a flow boiling test facility to obtain dynamic and time-averaged void fractions in a horizontal tube. A series of evaporation tests have been run for two refrigerants. R-22 was tested under mass velocity conditions of 70, 100, 150 and 200 kg/m^2 s and R-410A for 70, 150, 200 and 300 kg/m^2 s in a 13.6 mm diameter glass tube. Using our newly developed image processing system, about 227 000 images have been analyzed in this study to provide the same number of dynamic void fraction measurements. From these images, 238 time-averaged void fraction values have been obtained for vapor qualities from 0.01 to 0.95. These experimental points show very good agreement with the horizontal version of the Rouhani–Axelsson drift flux void fraction model.

Keywords: Void fraction; Two-phase flows; Flow boiling; Stratified flows; Wavy flows; Heat transfer

1. Introduction

Significant advances in modelling of intube evaporation and intube condensation have been made by the introduction of flow pattern regime-based logic into heat transfer prediction models. These flow pattern based methods provide much higher accuracy than older ones through the use a heat transfer model specific to the particular flow pattern. Thus, a good representation of the two-phase interfacial flow structure, an accurate prediction of the void fraction, and a reliable flow pattern map are basic requirements for the continued development of these heat transfer models. In response, as shown in Part I of the current paper, a new optical technique has been

* Corresponding author. Tel.: +41-21-693-5981; fax: +41-21-693-5960.
E-mail address: john.thome@epfl.ch (J.R. Thome).

0301-9322/$ - see front matter
doi:10.1016/j.ijmultiphaseflow.2003.11.009

developed that simultaneously allows flow pattern observations and dynamic void fraction measurements to be made inside tubular sight glasses in stratified types of flow. Coupling this system to a test facility for experimental studies on intube flow boiling, concurrent measurements of heat transfer coefficients, two-phase flow pressure drops, flow patterns and void fractions are now feasible.

Existing void fraction models can be classified as either homogeneous or separated flow models. The homogeneous model assumes that the liquid and the vapor phases have the same velocities. The homogeneous void fraction model is reasonably accurate only for bubbly and mist flows, where the entrained phase travels at nearly the same velocity as the continuous phase. Separated models assume that the two phases travel at two different mean velocities. This approach is used by both analytical and semi-empirical methods. In the analytical theories, some quantity such as momentum or kinetic energy is minimized to obtain the velocity ratio between the mean velocities of the gas and liquid phases. Two examples are the momentum flux model and the Zivi (1964) kinetic energy model for which the velocity slip ratio S equals $(\rho_L/\rho_G)^{1/2}$ and $(\rho_L/\rho_G)^{1/3}$, respectively. The drift flux model accounts for non-uniformities in the velocity and void profiles across the flow channel and has the general form of, restricting its application to $\varepsilon > 0.1$:

$$\varepsilon = \frac{x}{\rho_V}\left[C_0\left(\frac{x}{\rho_V}+\frac{1-x}{\rho_L}\right)+\frac{\langle u_{GU}\rangle}{G}\right]^{-1} \tag{1}$$

This is an analytical expression applicable to any two-phase flow regime and takes into account the effects of non-uniform flow through the parameter C_0 and the effect of local relative velocity through the weighted mean drift velocity $\langle u_{GU}\rangle$.

Rouhani and Axelsson (1970) proposed the following factors for the drift flux model for vertical flows:

$$\langle u_{GU}\rangle = 1.18(1-x)\left[\frac{g\sigma(\rho_L-\rho_V)}{\rho_L^2}\right]^{0.25} \tag{2}$$

$$C_0 = 1+0.2(1-x)\left(\frac{gd_i\rho_L^2}{G^2}\right)^{0.25} \tag{3}$$

The Rouhani–Axelsson void fraction model was later modified by Steiner (1993) for application to horizontal flows

$$\varepsilon = \frac{x}{\rho_V}\left[(1+0.12(1-x))\left(\frac{x}{\rho_V}+\frac{1-x}{\rho_L}\right)+\frac{1.18(1-x)[g\sigma(\rho_L-\rho_V)]^{0.25}}{G\rho_L^{0.5}}\right]^{-1} \tag{4}$$

Steiner (1993) did not provide a comparison of Eq. (4) to void fraction data but only noted that he found it to work for R-12 and R-22. Kattan et al. (1998b) used this expression in their two-phase flow heat transfer model. Recently, Thome and El Hajal (2002) proposed application of the Rouhani–Axelsson model in their flow pattern prediction map rather than the original method of Taitel and Dukler (1976) used by Kattan et al. (1998a). This provides a simpler method for calculating the transitions and gives equivalent results. It must also be mentioned that this void fraction model includes the effects of mass velocity and surface tension, which are missing in many other analytical and semi-empirical methods.

The objectives of the present study were to obtain a large number of accurate void fraction measurements over the entire range of vapor quality for different mass velocities and different fluids, and then compare them with Eq. (4) used in the heat transfer model of Kattan et al. (1998b). As noted in Part I, the technique is limited to stratified types of flow without significant vapor entrainment in the liquid and vice versa, which are typical of refrigerant flows.

2. Test facility

Fig. 1 shows a simplified layout of the refrigerant test loop, with a close up view the void fraction measurement set-up. The refrigerant first passes through a series of horizontal electrical preheaters and then through an insulated tube without any sharp elbows. Then, the refrigerant enters the tubular test section and is heated by counter-current flow of hot water in the annulus of the double pipe system. The void fraction is measured at the outlet of the test section as shown and the refrigerant then goes through a condenser, a magnetically driven gear type of pump (oil free) and finally, a Coriolis mass flow meter together with its inlet and outlet temperatures. The circuit also includes a vapor–liquid reservoir for controlling the amount of refrigerant in the circuit and thus the operating pressure. The hot water flow rate in the annulus is measured with another calibrated Coriolis mass flow meter.

The test section is made of copper and has a plain, smooth interior with an internal diameter of 13.84 mm, and a heated length of 2.026 m. The outer stainless steel annulus has an internal

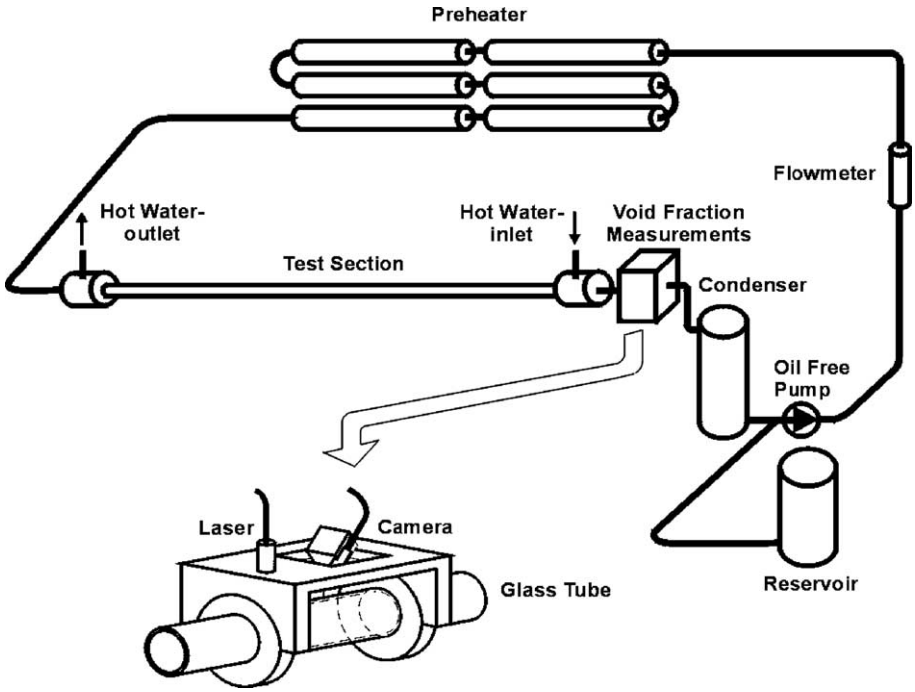

Fig. 1. Flow boiling test facility with the void fraction measurement system.

diameter of 20 mm and a wall thickness of 1.5 mm. The test section was well insulated to prevent heat gains from the surroundings.

A complete schematic diagram of the heat transfer test section is shown in Fig. 2. The refrigerant enters the copper tube at the left and leaves at the right, and flows into the sight glass with a smooth transition in tube diameter from 13.84 to 13.60 mm of the sight glass. The hot water enters the annulus at the right and leaves at the left. Four thermocouples at the inlet (123, 124, 125, 126) and four thermocouples at the outlet (101, 102, 103 and 104) are used to measure the respective mean inlet and outlet temperatures of the water. The inlet and outlet temperatures and pressures of the refrigerant are obtained as well. Energy balances over the preheater and test section give the vapor quality of the flow that enters the sight glass tube used for the void fraction measurements.

All thermocouples were carefully and accurately calibrated to an accuracy of ±0.02 °C compared to the precision thermometer of Omega Engineering, model DP251. The saturation temperature was calculated from the measured saturation pressure using the EES program and verified with two thermocouples that measure refrigerant temperature at the inlet and outlet of the test section. The accuracy of pressure transducers was ±20 mbar. A computerised data acquisition system was used to record all data and to insure that steady-state conditions were reached. The criteria for steady-state conditions is the refrigerant saturation temperature, which should not change more than ±0.05 °C during one acquisition.

To be sure that the entire measurement system is working correctly, liquid–liquid tests have been done with R-22 and R-410A versus water to determine the accuracy of the energy balance

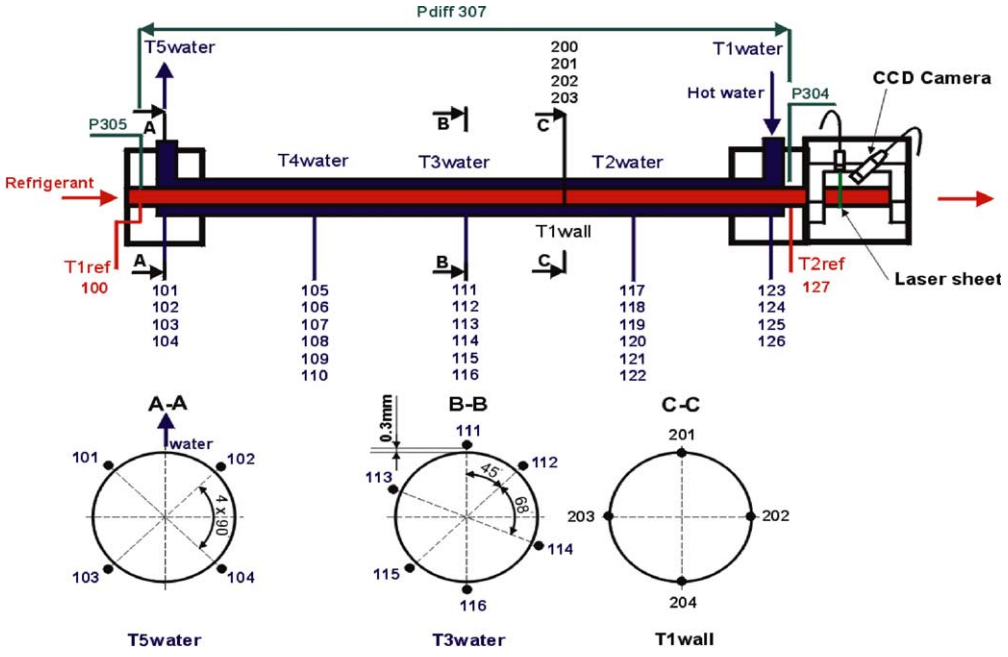

Fig. 2. Test section of the flow boiling test facility with the void fraction measurement set-up (cross-section A–A: water thermocouple alignment in heads of test section; cross-section B–B: water thermocouple alignment in the three central positions; cross-section C–C: wall thermocouple alignment in the heat transfer measurement position).

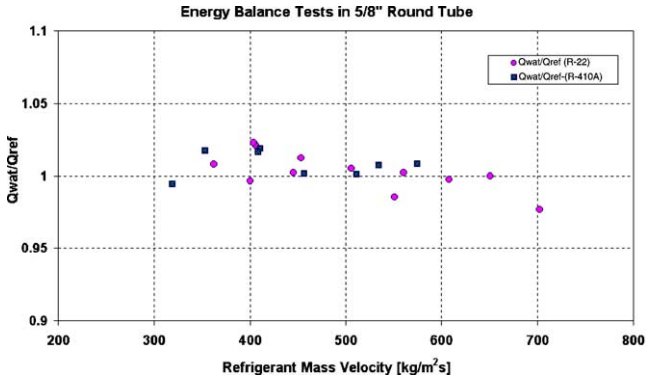

Fig. 3. Energy balance in the liquid–liquid tests for refrigerants R-22 and R-410A.

between the heating and cooling fluids and hence that when evaporating refrigerant. As one can see in Fig. 3, Q_{wat}/Q_{ref} varies from 0.98 to 1.02, with a mean error of ±0.98% for R-410A and ±0.96% for R-22. This is very accurate for these types of measurements and means the local vapor quality entering the sight glass is known within ±1% on average (±2% maximum error).

For the void fraction measurements, the upper support described in Part I is used. The video camera and the laser optic fibre head are fixed on it in the same manner as they were during the calibration procedure. The sight glass is a borosilicate glass tube with an external diameter of 16 mm and a wall thickness of 1.20 mm. It has a very good degree of roundness (±0.02 mm) and very good optical qualities according to DIN ISO 3585. The camera is equipped with a video card TARGA 2000, which allows a real time acquisition rate of 25 frames per second with an image resolution of 720×576 pixels. Because of the interlaced acquisition mode (i.e. even lines and odd lines are not exposed and not recorded at the same time), a resampling procedure is performed. The resampling technique consists of segregating even lines from odd lines and recalculating the respective missing lines with a linear interpolation. This operation yields two images from one, increasing artificially the acquisition rate to 50 frames per second and removes the "shadow" effect of interlaced images to achieve sharp interfacial contrast. The calibration procedure described in Part I is simply repeated over both image types (i.e. over the images issued from even lines and from odd lines respectively).

3. Void fraction measurements

3.1. Experimental conditions

Experimental tests have been run for two refrigerants at four mass velocities over nearly the entire range of vapor quality ($0.01 \leqslant x \leqslant 0.95$). R-22 was tested at mass velocities of 70, 100, 150 and 200 kg/m^2 s and R-410A for 70, 150, 200 and part of the range for 300 kg/m^2 s. The saturation temperature was 5 °C and the heat fluxes in the heat transfer section ranged from 2.0 to 7.5 kW/m^2 (low heat fluxes were used to avoid nucleate boiling and its entrained bubbles in the flow). The minimum heat flux was applied especially for the lower void fractions measurements to obtain low

vapor qualities at the outlet of the heat transfer test section. After reaching a steady-state condition, the cross-sectional image sequences were simultaneously acquired with all the heat transfer parameters. At each mass velocity, these acquisitions were repeated for 25–37 different vapor qualities. For each case, the acquisition time was between 18 and 20 s and provided 900–1000 images, that were then used to give a time-averaged void fraction value at each test condition.

The images were processed on a PC with a Pentium 3 processor (455 MHz) as described in Part I of this paper. All together, 238 experimental points have been acquired corresponding to almost 227 000 images. Due to optical perturbations, some sequences had to be removed. The best image quality in terms of the contrast between the vapor and the liquid phase is obtained at low vapor qualities and low mass velocities (i.e. for low liquid phase velocities). On the other hand, at high vapor qualities, occasionally some droplets of liquid were carried away by the high velocity vapor, which resulted in additional reflections and secondary refraction of the light. Moreover, for high vapor quality tests, the rhodamineB powder deposited on the upper "dry" internal perimeter of the tube. As a result, very intense white spots sometimes appear on the acquired image (over-exposed images). This problem is partially avoided by regularly washing the tube wall with high frequency waves at higher mass velocities before returning to the test conditions. Finally, condensation of the moisture in the room air that appears on the external surface of the tube was removed with a dry air jet to avoid blurred image acquisition.

3.2. Results and discussion

Each test case of void fraction measurement can be presented as a function of time, but due to the high number of measurements, only a few cases are shown here. The first case is for a R-410A stratified-wavy flow (Fig. 4) with the void fraction of each sequential image plotted versus time. The mass velocity is $G = 70$ kg/m^2 s and vapor quality is $x = 0.2$. The characteristic cyclic vari-

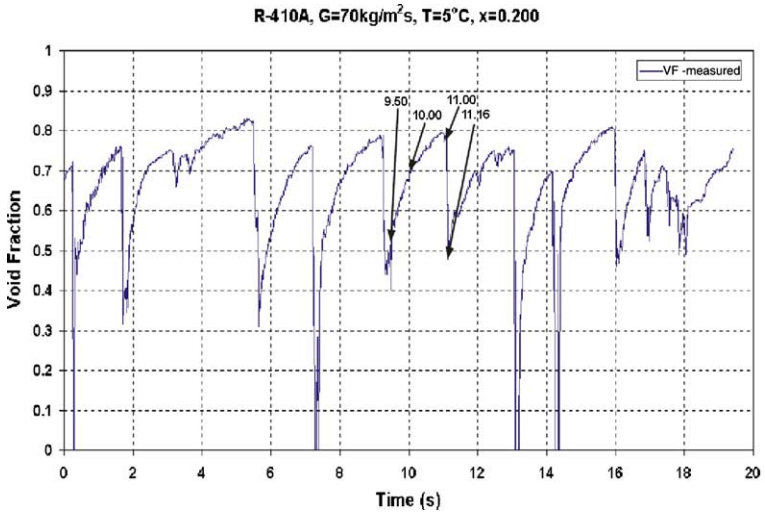

Fig. 4. Void fraction evolution for stratified-wavy flow with intermittent liquid: R-410A, $G = 70$ kg/m^2 s, $T = 5$ °C, $x = 0.2$.

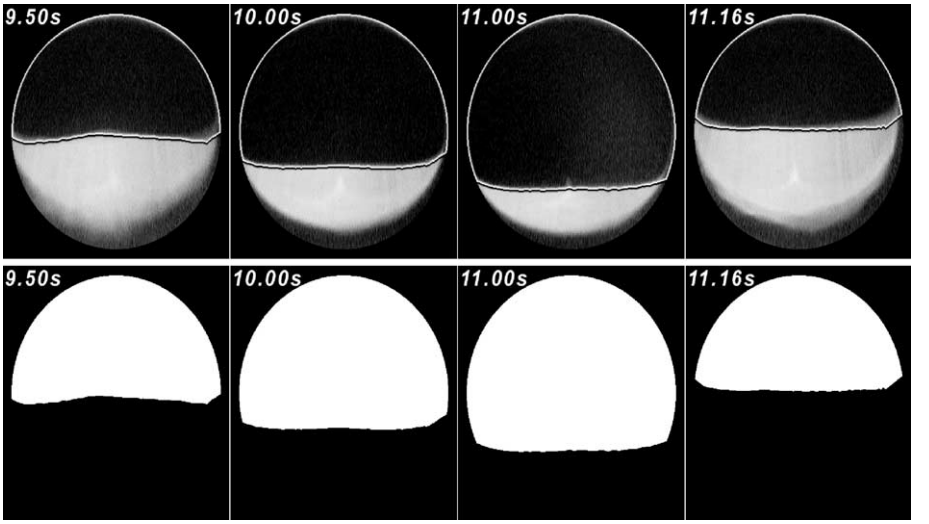

Fig. 5. Variation of the liquid interface during one wave cycle (from 9.50 to 11.16 s): R-410A, $G = 70$ kg/m^2 s, $T = 5$ °C, $x = 0.2$. Transformed images with detected interface (upper part) and final processed images used for void fraction calculation (bottom part).

ation observable corresponds to waves passing through the cross-section and the time in-between corresponds to their period. The void fractions equal to 0.0 represent the passage of liquid slugs that fill the entire channel. Fig. 5 shows cross-sectional images within the time interval of 9.50–11.16 s, which correspond to passage of a wave with respective void fractions of 0.537, 0.685, 0.794 and 0.479. There are two groups of images corresponding to two different steps of the image processing. The first group (top) is obtained after optical transformation and interfacial detection (black curves). As can be seen, the position of the interface is precise and parameters like the dry angle and the liquid height can be very accurately determined. The second group (bottom) illustrates the final black and white processed images used for void fraction calculation. The cross-sectional area below the gas/liquid interface is filled with black color and represents the liquid phase. Inversely, the white color corresponds to the gas phase. The cross-sectional void fraction is thus calculated from the ratio of the white pixels to the total number of pixels of the channel.

The second case is presented in Fig. 6 for slug flow with R-410A. The mass velocity is $G = 150$ kg/m^2 s and vapor quality is $x = 0.103$. The interfacial profile variations are more rapid compared to the previous case. Indeed the periods of waves are shorter and the whole tube perimeter is wetted more frequently by liquid slugs. The recorded sequence contains about 20 large amplitude wave passages that should give a good representation of the time-averaged void fraction value.

The transformed images in the upper part of Fig. 7 depict specific cross-sectional views due to passage of a liquid slug. For this very high frequency phenomenon (only 0.06 s between first and last image), the dynamic interface detection between gas and liquid remains accurate, even if a very small vapor zone has not been detected (the ''tooth'' in the 2.82 s image in the upper group). Concerning the same image, the interface detected seems to be very rough, especially close to the internal tube surface at the right side. The surface detection technique is directly based on the absolute luminance signal. If the distinction of the interface is locally perturbed by a shadow (issued from a rhodamineB deposit or from a moisture droplet), the detection will be directly

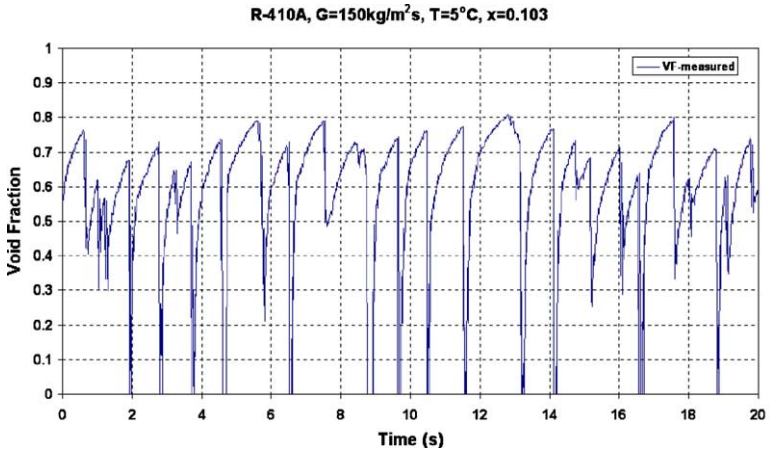

Fig. 6. Void fraction distribution for slug flow: R-410A, $G = 150$ kg/m^2 s, $T = 5$ °C, $x = 0.103$.

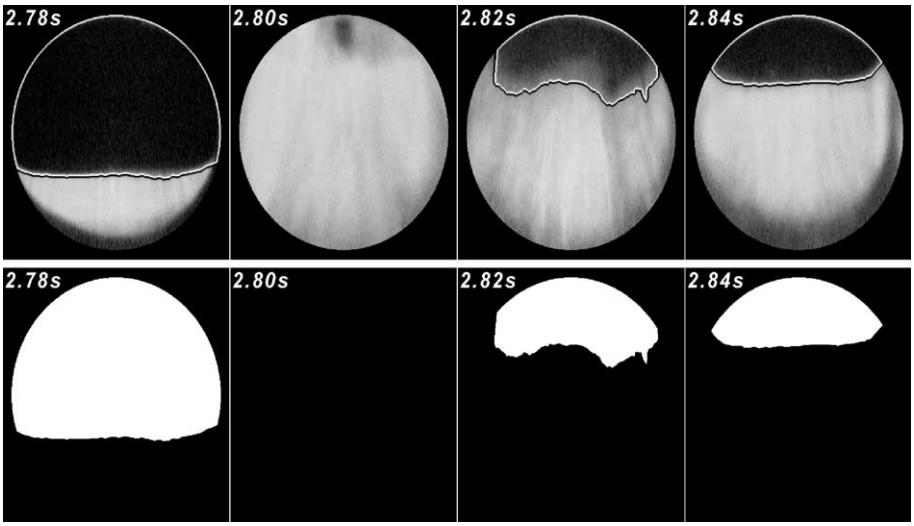

Fig. 7. Variation of the liquid interface for slug flow: R-410A, $G = 150$ kg/m^2 s, $T = 5$ °C, $x = 0.103$. Transformed images with detected interface (upper part) and final processed images used for void fraction calculation (bottom part).

influenced and such a rough interface (which probably has no fluid dynamic sense) will appear. A smoothing function could be applied on the interface profile to eliminate these minor anomalies, but the influence in terms of void fraction measurement error is very low, and thus the technique remains very accurate without such an intervention. Concerning the lower images in Fig. 7, the corresponding black-and-white processed images used to identify the surface of the vapor zone is shown, which are used for the void fraction calculation.

Reviewing the literature, nearly all slug flow length and frequency data and prediction methods are for air–water and air–oil adiabatic flows, which are quite different that the current test conditions, chosen specifically for examining evaporating flows of refrigerants, e.g. a widely used

industrial process in refrigeration and air-conditioning systems. Extrapolating the method of Tronconi (1990) for instance to the present conditions, where his slug frequency ω is predicted to be

$$\omega = 0.61 \frac{\rho_V u_V}{\rho_L h_V} \tag{5}$$

it overpredicts a sampling of slug frequencies, deduced from our measurements, by a factor of 2–3. As air–water dry angles are quite different than those for the two refrigerants (see Part I), this is not surprising. Hence, one can conclude that air–water data and prediction methods for dry angles and slug flows are not representative for typical working fluids (refrigerants and hydrocarbons) that have much lower surface tensions and contact angles.

Based on the 238 image sequences obtained experimentally, 238 time-averaged values of void fraction were determined. The results obtained for R-22 and R-410A are shown in Figs. 8 and 9, respectively. The experimental time-averaged void fractions are presented as a function of vapor quality and are compared with the homogenous model (for reference only) and with the Steiner version of the Rouhani–Axelsson drift-flux model.

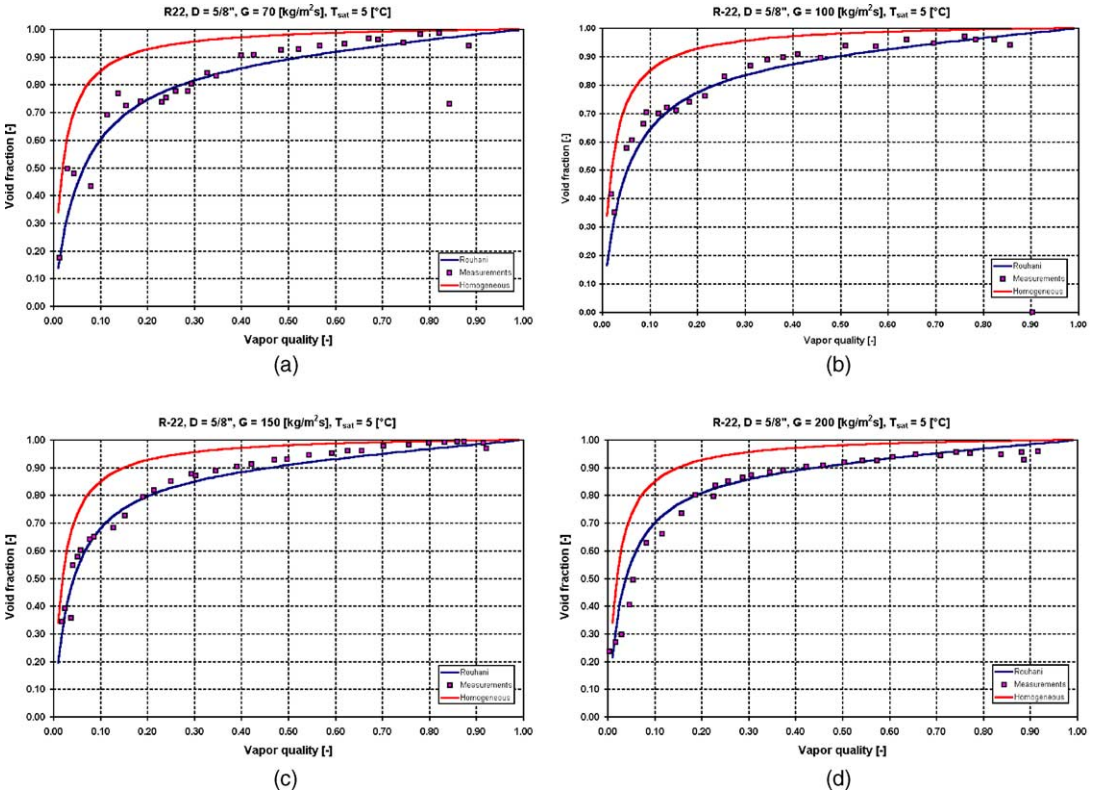

Fig. 8. Evolution of the void fraction as a function of vapor quality for R-22 at four mass velocities: (a) 70, (b) 100, (c) 150 and (d) 200 kg/m^2 s.

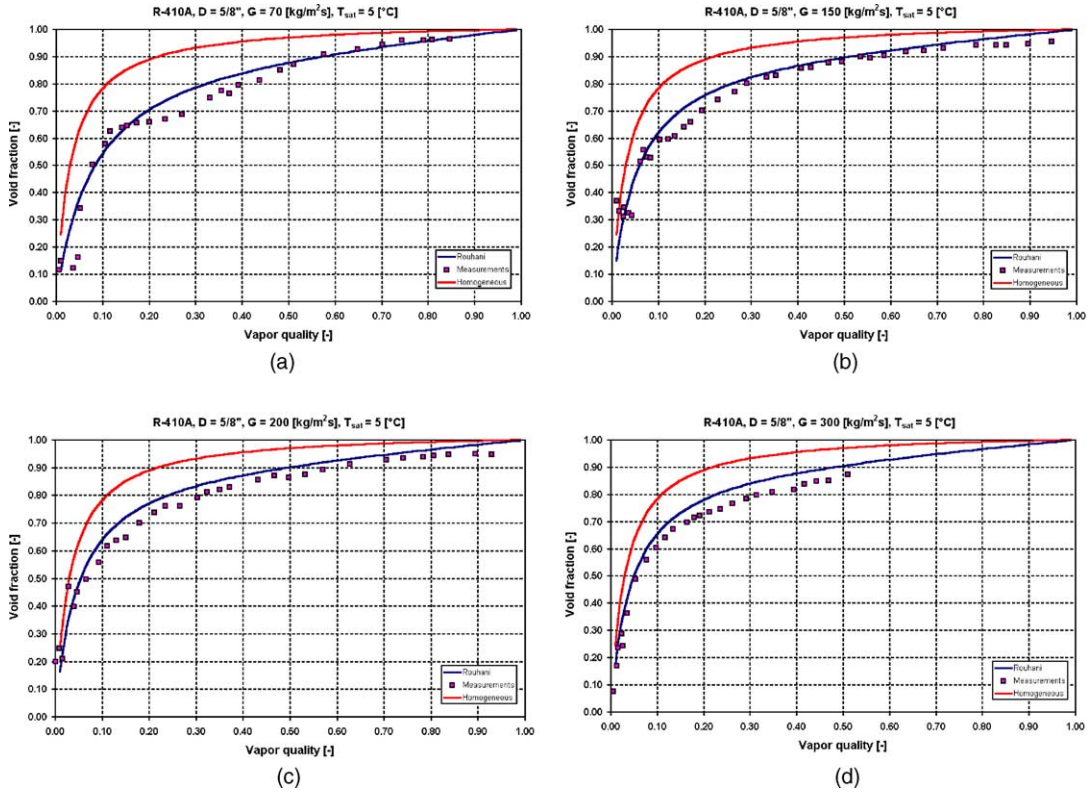

Fig. 9. Evolution of the void fraction as a function of vapor quality for R-410A at four mass velocities: (a) 70, (b) 100, (c) 200 and (d) 300 kg/m^2 s.

As can be seen in Figs. 8 and 9, the experimental optical measurements of time-averaged void fraction closely follow those predicted by the Steiner version of the Rouhani–Axelsson model for horizontal tubes and are always less than the void fraction values given by the homogeneous model, except for a few stray values at very low vapor qualities.

For the measurements at low vapor quality ($x < 0.1$), some successive points present a discontinuous evolution of time-averaged void fraction, especially for measurements at low mass velocity ($G = 70$ kg/m^2 s for R-22 and R-410A, Figs. 8(a) and 9(a) respectively). For example, refer to the values of $x \approx 0.05$ in Fig. 9(a), which are too low relative to expectations. Two specific parameters can explain such deviations, a non-representative acquisition time period (an issue discussed below) and the maximum errors ±2% in energy balances.

Fig. 10 shows void fraction as a function of time for R-410A at $G = 70$ kg/m^2 s (a relatively low mass velocity) and $x = 0.051$. Two different trends appear on this graph and seem to be due to two different types of flows. The first is characterized by short slugs (each lasting about 0.5 s) and the second represents a long wave (lasting almost 4 s). The short slug phenomenon appears to repeat itself (beginning at time 13 s) with relatively small void fraction values, but the long wave phenomenon appears completely only one time within the sampling period in Fig. 10 with much larger values. This indicates that in this case, the measurement sampling period was too short to

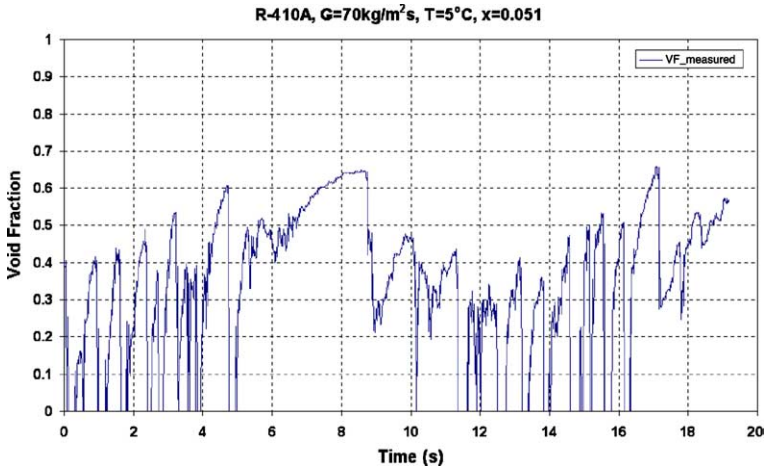

Fig. 10. Void fraction as a function of time for R-410A, $G = 70$ kg/m^2 s, $T = 5$ °C, $x = 0.051$.

capture several cycles of the repeating flow phenomena, yielding a time-averaged void fraction measurement below the real value in a video sequence dominated by the short slug phenomenon. However, as can be observed for higher mass velocity (Fig. 6, $G = 150$ kg/m^2 s, $x = 0.103$) or for higher vapor quality (Fig. 4, $G = 70$ kg/m^2 s, $x = 0.20$) the acquisition time of 18–20 s is sufficient to obtain a good representation of their time-averaged void fraction values. Nevertheless, despite the fact that the use of the Rouhani–Axelsson drift flux correlation is recommended for void fractions higher than 0.1, the experimental values over all void fraction values agree quite well with those calculated by this model, especially for R-410A and $G = 300$ kg/m^2 s (Fig. 9(d)), where almost all points perfectly follow the model curve in the void fraction range from 0 to 0.1.

Considering vapor quality values between 0.1 and 0.3 in Fig. 9, void fraction seems to be systematically over predicted compared to Eq. (4) and exhibits a deflection in its trend. In fact, one can observe that all temporal measurements of void fraction in this range of vapor quality show a transient situation between the passage of rapid slugs (wetting the total internal circumference of the tube) and the passage of rapid waves (e.g. as in Fig. 4). Therefore, these observations seem to identify a transition zone (depending on G since the limits are not exactly the same for all measurements) between a slug flow and a stratified wavy flow.

As noted earlier, for tests at high vapor quality (where $x > 0.4$), deposition of rhodamineB on the internal surface of the tube produced some spurious bright spots on the acquired images. These intense white spots disturbed the interface detection process and they were very often identified incorrectly by the image processing program as a limit of the liquid phase. Because the spots are systematically located on the "dry" upper perimeter of the tube, when this deposition occurs the resulting void fraction measurements tend to yield lower time-averaged values than the actual ones (images with such spots tend to give void fractions of about zero). These difficulties start to appear at $x \approx 0.5$, and become much more important for $x > 0.9$. Thus, for some tests, a filtering procedure of the results was required to remove these spotted images. To do this, a void fraction threshold is fixed by optically analysing the superposition of the transformed images and the respective detected interfaces (like the images in the upper series of the Figs. 5 and 7). Below the threshold, all the results are automatically suppressed. Fig. 11 shows the void fraction

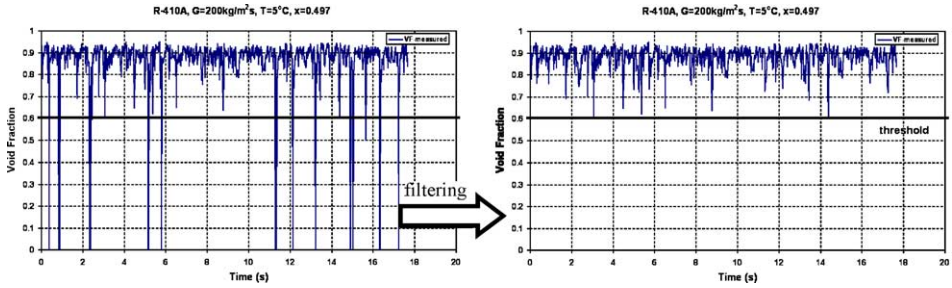

Fig. 11. Filtering of void fraction signal for R-410A, $G = 200$ kg/m^2 s, $T = 5$ °C, $x = 0.497$.

distribution before and after such filtering for R-410A, $G = 200$ kg/m^2 s and vapor quality $x = 0.497$. In this case, the void fraction threshold was set at 0.6 and only 21 values have been deleted (no liquid slugs occupying a large fraction of the channel are seen visually in these flows and hence it is clear that these 21 images do not represent the flow but only occasional ''sparkling'' on the upper perimeter). The most intensive filtering was required for vapor qualities above 0.9. For these test conditions, the fraction of the remaining liquid phase is extremely small and the deposition of rhodamineB from evaporated refrigerant forms a thin layer on the upper dry perimeter of the glass tube. Therefore, the highest void fraction threshold used was 0.9 and in the worst case only 25% of the images were suitable for the mean void fraction calculation (i.e. about 250 images).

The last case discussed here concerns the R-410A measurements at $G = 300$ kg/m^2 s. Contrary to all the other tests, the time-averaged void fraction measurements for $x > 0.2$ are noticeably less than those calculated with (4). Moreover, due to the quality of the images, the image processing was stopped for $x > 0.5$. The reason was the type of flow, i.e. annular. In fact, for $x < 0.5$, an annular flow was already present, but the film thickness was too thin to be detected by the image processing. By viewing the original image sequences, it is possible to imagine an annular flow, because local deposits of rhodamineB with their characteristic white spots are immediately washed away by the flow. However, at this mass velocity and for $x \approx 0.4$, the flow field is clearly not characterized by slugs nor by stratified wavy flow. The internal surface of the tube is washed only in the presence of an annular flow. Thus, the presence of a thin liquid film modifies the optical reflection of light through the glass tube and as a result, the interface is incorrectly measured as being higher than it actually is. Consequently, the measured void fraction is slightly lower than the real value. Concerning the images for $x > 0.5$, either they appear completely blurred or the image processing detected a liquid film at the top and the measured void fractions tend to zero, which is not feasible. As noted in Part I, the present method is not currently applicable to annular flow, nor to slug flows with significant entrainment of bubbles, and neither when bubbles support a liquid film on the upper perimeter.

4. Conclusion

A new optical method has been used to measure dynamic and time-averaged cross-sectional void fractions simultaneously with heat transfer coefficients and pressure drops in flow boiling of

two refrigerants. The measurements confirm that the horizontal tube version of drift-flux model of Rouhani–Axelsson accurately predicts the void fraction distribution as a function of vapor quality, even at void fractions less than 0.1. Therefore, the choice of the Rouhani–Axelsson model to calculate void fraction is very appropriate for use with the Kattan et al. (1998a,b) flow boiling heat transfer model and map. This new technique also provides valuable information about flow structures as a function of time for different mass velocities and vapor qualities. These results will be used to further improve our two-phase heat transfer model by using the void fraction and dry angle data to analyze the corresponding flow boiling data measured during these same tests.

Acknowledgements

These investigations were supported by the Swiss National Fund (FNS) contract number 21-57210.99 and by the Air-Conditioning and Refrigeration Technology Institute (ARTI) contract number 605-20040.

References

Kattan, N., Thome, J.R., Favrat, D., 1998a. Flow boiling in horizontal tubes: Part 1—Development of a diabatic two-phase flow pattern map. J. Heat Transfer 120, 140–147.

Kattan, N., Thome, J.R., Favrat, D., 1998b. Flow boiling in horizontal tubes: Part 3—Development of a new heat transfer model based on the flow pattern. J. Heat Transfer 120, 156–165.

Rouhani, S.Z., Axelsson, E., 1970. Calculation of void volume fraction in the subcooled and quality boiling regions. Int. J. Heat Mass Transfer 13, 383–393.

Steiner, D., 1993. VDI-Wärmeatlas (VDI Heat Atlas) chapter Hbb. In: Verein Deutscher Ingenieure, editor. VDI-Gesellschaft Verfahrenstechnik und Chemieingenieurwesen (GCF), Translator: J.W. Fullarton, Düsseldorf.

Taitel, Y., Dukler, A.E., 1976. A model for predicting flow regime transitions in horizontal and near horizontal gas–liquid flow. AIChE J. 22, 47–55.

Thome, J.R., El Hajal, J., 2002. Two-phase flow pattern map for evaporation in horizontal tubes: Last version, In: 1st International Conference on Heat Transfer, Fluid Mechanics, and Thermodynamics, HEFAT 2002.

Tronconi, E., 1990. Prediction of slug frequency in horizontal two-phase slug flow. AIChE 36, 701–709.

Zivi, S.M., 1964. Estimation of steady-state steam void fraction by means of the principle of minimum enthropy production. Trans. Am. Soc. Mech. Eng., Ser. C, J. Heat Transfer 86, 247–252.